



ANALYZING FREQUENCY RESPONSE ANALYSIS EXPERIMENTALLY FOR BONE HEALING DETECTION: EXAMINING THE POTENTIAL OF VIBRATIONAL EVALUATIONS

Abbas Jawad KADHIM ^{*} , Mohammed Jawad AUBAD , Ameen M. AL-JUBOORI

Mechanical Engineering Department, College of Engineering, University of Babylon, 51001 Babylon, Iraq

^{*} Corresponding author email: mengabbas@gmail.com

Abstract

Assessment of bone healing is essential for efficient orthopedic treatment. This work investigates the feasibility of assessing frequency response experimentally for bone healing detection, with a particular emphasis on the use of vibrational assessments. Detailed experimental studies were carried out to determine the ability of frequency response analysis to assess bone healing. Mechanical excitation was delivered to cracked bone samples at various frequencies, and the vibrational responses of the displacement and accelerations were measured. The experimental setting includes testing five samples, to cover a wide range of possibilities. The obtained vibrational, such phase, magnitude, and coherence, were examined to find common patterns and changes linked with the healing process. The results showed that frequency response analysis has the potential to identify bone healing, as unique vibrational responses were seen in healed samples under cyclic load for different turns (0, 1000, 2000, 3000, and 4000). The findings demonstrate the sensitivity of vibrational evaluations in capturing the mechanical properties and healing condition of bone tissue. Furthermore, the presence of cracks impacts both structural integrity and natural frequency. Natural frequency decreases as the number of cycles increases. The highest frequency reduction occurred at the first mode shape and maximum cycle number, indicating considerable fracture behaviour changes. Natural frequency can be used to assess bone health; higher stiffness and frequency are associated with smaller crack size.

Keywords: Bone healing detection, signal analysis, natural frequency, vibration analysis, dynamic characteristics

List of Symbols/Acronyms

FFT – Fast Fourier Transform;

l – distance [mm];

Δ – measurement tolerance [mm].

1. INTRODUCTION

Vibration techniques have emerged as a significant tool in orthopedics and rehabilitation for assessing bone repair. These technologies offer objective, non-invasive means to evaluate and follow the progression of bone healing, providing critical information about the process and guiding treatment decisions. These strategies can help with recovery monitoring and assessment. Compared to more invasive and subjective traditional procedures such as X-rays and manual palpation, vibration-based approaches provide a quantitative assessment that is easy to repeat over time. This allows for precise monitoring of the bone-healing process, making it easier to detect healing early and respond appropriately when necessary. Second, vibration techniques can provide valuable information on the

rate and quality of fracture healing by assessing the mechanical characteristics of the healed bone. It is possible to gain quantitative information regarding the mechanical behavior of the healing bone by analyzing factors such as resonance frequency, damping coefficient, and wave propagation qualities. This facilitates the tracking of the healing process and provides medical practitioners with the necessary information to determine the best course of action. Furthermore, the process of developing a treatment plan for bone healing is primarily reliant on vibration-based assessments. Clinicians can determine whether weight-bearing, physical therapy, or surgery is the best course of action by objectively monitoring the healing process. Healthcare practitioners can optimize therapy and improve outcomes by developing individualized strategies for each patient. Several researches have looked into the use of mechanical vibration analysis to evaluate bone healing and integrity. Anderson et al. (2020) repurposed a low-power, miniature tire-pressure sensor (FXTH87) for measuring load and deformation in orthopaedic and biomedical

applications. They modified the capacitive transducer membrane and embedded the sensor in a deformable enclosure. The sensor required $350 \pm 24 \mu\text{m}$ of compressive deformation to reach its maximum output signal, accurately predicting applied loads up to 35 N. The FXTH87 sensor effectively senses and transmits load-induced deformations, offering a precise means to monitor deformation and load within small-scale, deformable enclosures. Atte Joutsen et al. (2020) developed and validated a prototype device using vibration analysis to measure sternal bone connectivity post-sternotomy. The device distinguished between intact bone, precise wire fixation, and fixation with a gap. While further studies are needed to confirm its accuracy, the method shows potential for early detection of bone separation to prevent complications. Sorriento et al. (2021) developed a capacitive device for monitoring bone fracture healing by measuring the displacement of external fixator pins. The system provides non-invasive, repeatable assessments of implant stability and bone callus stiffness with a 0.5 mm and 0.5° resolution in 3D space. Ke Zou et al. (2022) reviewed the role of uncertainty estimation in deep learning for medical imaging. They examined aleatoric and epistemic uncertainties, their estimation methods, and recent advances in deep learning models that incorporate these estimations. The paper highlights the importance of uncertainty estimation for enhancing the reliability of AI systems in healthcare, identifying areas of concern, and informing clinicians. It also addresses challenges and future directions in this field, aiming to advance research and application in medical imaging. Song et al. (2022) studied bone damage during Kirschner wire drilling by analyzing the effects of drilling parameters on force, temperature, and bone damage. They found that lower temperatures do not always reduce damage and recommended using lower rotational speeds, lower bevel angles, and higher feed rates to minimize thermal damage, force, and burrs. Arpinar et al. (2005) did a study to assess bone strength by employing vibration analysis and dual energy x-ray absorptiometry (DEXA). The researchers conducted a comparison between bone mineral density measured by DEXA and the results of modal analysis. This comparison indicated a possible method for forecasting bone strength. Christopoulou et al. (2006) evaluated the effectiveness of modal damping as a diagnostic factor for osteoporosis. A link was discovered between modal damping and trabecular bone density, suggesting that modal damping can serve as a diagnostic tool for osteoporosis and as a means to assess bone repair. Gregory N. (2008) employed frequency analysis to assess the soundness of elongated bones, specifically focusing on the spinal column. The researchers showcased how frequency

response functions are highly responsive to alterations in bone structure, indicating their potential as a diagnostic instrument. Bediz (2010) used vibration analysis to assess changes in the structural dynamic characteristics of the human tibia. The researchers discovered that the resonant frequency of the tibia reduced as the bone mineral density decreased. They proposed that modal damping could serve as a diagnostic technique for metabolic bone illnesses and the healing of bone fractures. Van Engelen (2012) conducted a study that aimed to forecast the mechanical characteristics of human lumbar motion segments through the use of vibration analysis. A robust association was discovered between vibration analysis and quasi-static mechanical testing, suggesting that vibration analysis can be effectively employed to assess the mechanical characteristics of human lumbar motion segments. In their study, Campoli et al. (2014) examined the correlation between the distribution of bone density, bone form, and bone resonant frequency (RF). The researchers created finite element models and observed fluctuations in the resonant frequency as a result of alterations in bone shape and density. This indicates that resonant frequency analysis has the ability to evaluate bone characteristics. Mattei et al. (2016) examined the change in the inherent frequency of fixation structures as they recover to assess the process of bone fracture healing. The researchers employed vibration analysis and observed a rise in the natural frequency as the fractured bone underwent healing. This discovery offers valuable information for evaluating the healing process of fractures. Mattei et al. (2017) conducted a study on fractures that were treated with external fixators. They devised a test procedure that involved impact tests to assess and describe the properties of the treated bone. They discovered that fixators and pins have the ability to alter the bone's frequency response, which suggests the process of healing. Di Puccio et al. (2017) introduced a system for detecting bone repair using vibrational techniques. They detected fluctuations in resonant frequencies on a biweekly basis, enabling more frequent surveillance in comparison to X-ray. Di Puccio et al. (2017) conducted a separate study where they analyzed fractures that were treated with external fixators. They specifically looked at how changes in resonant frequencies may be used to determine the stiffness of the bone-callus. The experimental modal analysis confirmed the efficacy of this approach for monitoring the healing of fractures. In their study, Mattei et al. (2018) introduced a vibration technique for monitoring the progress of femur healing when an external fixator is used. Periodic impact tests were done to assess the changes in resonance frequencies of the bone as the callus progressed from the soft phase to the woven bone. Verdenelli et al. (2018) employed vibrational

methods to analyze a human tibia both with and without an external fixation device. Modal parameters were compared, and a numerical model was created to interpret the experimental data. Mattei et al. (2019) showed that mechanical vibration is beneficial in assessing bone repair in living organisms. The researchers evaluated the progression of the healing process in a tibial fracture that was treated with a fixator by conducting impact tests. They noticed that the resonance frequencies of the fracture increased as time passed. Chiu et al. (2019) examined the use of vibrational analysis to track the progress of healing in a femur that was stabilized using a plate-screw. The researchers employed cross-spectrum and coherence analysis to objectively evaluate the different phases of the healing process. Mattei et al. (2021) employed a non-intrusive vibrational technique to evaluate the recovery of a complicated fracture that was managed with external fixation. They tracked the hardening of the callus and saw a rise in resonance frequencies as the healing progressed. Vien et al. (2022) performed a clinical investigation and discovered a correlation between certain modal frequencies and femur length, indicating their potential as quantitative indicators for bone health. The objective of this study was to test the practicality and dependability of the vibrational technique (frequency response) in quantitatively measuring the progress of healing in a cracked bone. The frequency response results along with, phase, magnitude, and coherence were also determined and examined carefully. The effect of crack of the natural frequencies of the five modes of the bone was also addressed.

2. EXPERIMENTAL SETUP

An experimental setup for the frequency response measurements of the bone presented in the current work will be explained in the chapter. The setup typically consists of a specific mechanism designed for this work to produce a sinusoidal excitation force to the bone to excite its crack to initiate and propagate at different cycles, exciter and sensors to measure the dynamic characteristics of the bone at different values of the crack length.

During the experiment, the bone is subjected to impulsive dynamic input, and the response is measured at various cracks growths using sensors such as accelerometers. The response of the bone is then compared to the response of bone without cracks, and the effectiveness of frequency response for health detection of the bone is revealed.

The experimental test rig, in this work, was designed and developed in the laboratory of mechanical vibration of the university of Babylon belonged to the college of engineering. The experimental setup is presented in Fig. 1.

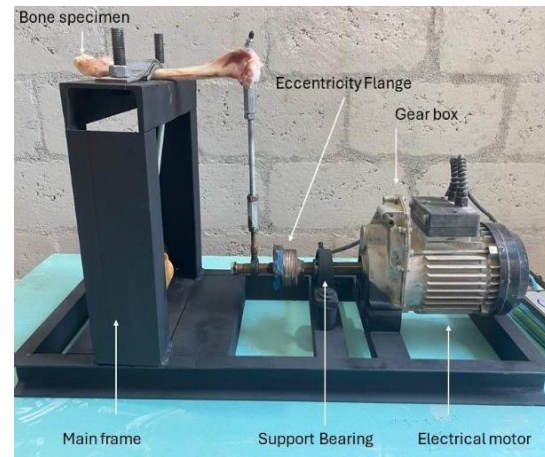


Fig. 1. Experimental Test-Rig

3. THE MAIN COMPONENTS OF THE TEST-RIG

The main steel frame is meant to hold up every element of the experiment. It serves as support for the gear box, the electrical motor, the supporting bearing, and the bone specimen. The electrical motor provide the required rotation motion which connected to the gear box to provide the required output power to achieve the fluctuating motion for the fatigue test. Gearboxes permit either a speed increase that raises the output speed while decreasing the torque or a speed decrease that increases the available torque [22].

In this work, speed decreasing and torque increasing are the main requirements to run the connecting link and provide the translational motion to the bone specimen. A specialized part that attaches to a shaft and permits eccentric or off-center rotational motion is called an eccentricity flange. It is made up of a flange that is purposefully offset or eccentric by being mounted onto the motor shaft in a way that deviates from the center axis. The translational motion provided by flange is twice the radius of eccentricity of the guiding shaft to the center of the main motor shaft. One can adjust this radius to produce the required translational motion. The connecting link in this work is as basic as bolts, nuts, and end bearings. The connecting links is designed to meet the requirements of the assembly, taking into account elements like alignment, adjustability, and load-bearing capacity. The link alignment is ensuring by adjusting to be perpendicular on both the guide link and the bone specimen.

3.1 Bone Specimen

Fig. 2 show bone specimen ready to be tested. The presence of crack will reduce the bone strength due to crack propagation and crack growth under uniform cyclic fatigue load.



Fig. 2. Bone Specimen

4. EXCITATION AND VIBRATION MEASUREMENT

4.1 Impulse hammer and accelerometers

Impulse hammer is used for providing the external excitation on the bone specimen. In Figure 3 (a), the impulse hammer type IH-01 is displayed. With a sensitivity of 25 mV/N, the excitation force is restricted to 200 N. The manufacturer offers four different kinds of hammer tips: stainless steel, hard plastic, aluminum, and soft rubber. The YMC161A accelerometer as shown in Figure 3(b) is used in this work. This kind of accelerometer was selected due to its frequency range of 1 Hz to 10 kHz, adhesive mounting, and light weight. A schematic showing how the sensors are connected to the bone is shown in Figure 3 (b).



(a) Impulse Hammer (b) Accelerometer type YMC161A

Fig. 3. Impulse hammer and accelerometers sensors

4.2 Dynamic Signal Analyzer

Figure 4 depicts the DSA type YMC 9004 that used in this work. It has four input channels. The signal acquisition and post-processing analysis for two types of working environments are supported by the YMC 9800 software.



Fig. 4. DCA type YMC 9004 [AAA]

Finally, to replicate the cantilever boundary conditions, the bone was fixed at one end to the supporting system and the free end is connected to the guide link by means of ball bearing as shown previously. To run the experiment, the accelerometer is directly attached to the bone specimen at specific location by using an adhesive glow. To determine the ideal locations for the accelerometer attachments, a flat surface survey was conducted on the bone. Once the bone is activated by the hammer, the accelerometer measures the signal and sends it to the Digital-to-Analog Converter (DAC) then to the programmable controller (PC) for signal analysis using Fast Fourier Transform (FFT) to determine the frequency response of the bone, as shown in Figure 5.



Fig. 5. Experimental setup

A range of regulated turns at preset revolution rates will be applied to every specimen. In steps of 1000 RPM, these rates will range from 0 RPM (revolutions per minute) to 6000 RPM (0, 1000, 2000, 3000, 4000, 5000, and 6000 RPM). At every turns, the specimen performance will be monitored and documented.

5. RESULTS OF SPECIMEN

5.1 Force and Acceleration Measurements

The amplitude of the impact force recorded by the load cell of the impact hammer is shown in the block diagram in Figure 6. The accelerometer is used to record the bone response in time domain. The force applied by the hammer is noticed to equal 100 N and required only 0.008 sec to diminish and distributed into the bone region. Similar behavior is noticed to the acceleration response. However, its response last longer than that corresponding of the excitation forces (0.016 sec), that is mainly due to the response wave speed that depends on the domain of the specimen (bone length) at which the accelerometers located.

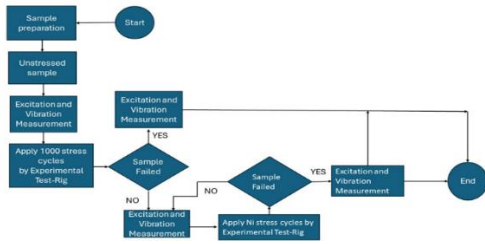


Fig. 6. A block diagram of the measurement system

5.2 FRF response and coherence response

The impulsive force and acceleration time response are used to determine the frequency response function (FRF). Figure 7 depicts a visualization of the FRF magnitude and test coherence. The magnitude peaks show the likely location of natural frequencies. Number of the peaks refers to the number of modes and natural frequencies. The phase angle diagram is used to detect the natural frequencies. An abrupt change in the phase angle diagram can reveal the natural frequency location. These locations feature peaks, but their magnitude is modest in comparison to the big magnitude peaks, and the size makes the little peaks undetectable (not considered peaks). The quality of the test is monitored using coherence. The coherence can be described as the relationship between stimulation and response. Coherence has values of one and zero. All tests must have a value close to one, and any test with low coherence values should be skipped. The lowest value of the coherence is 0.99925. This suggests that the reaction of the system is mostly determined by excitation, with noise sources having little effect on test findings.

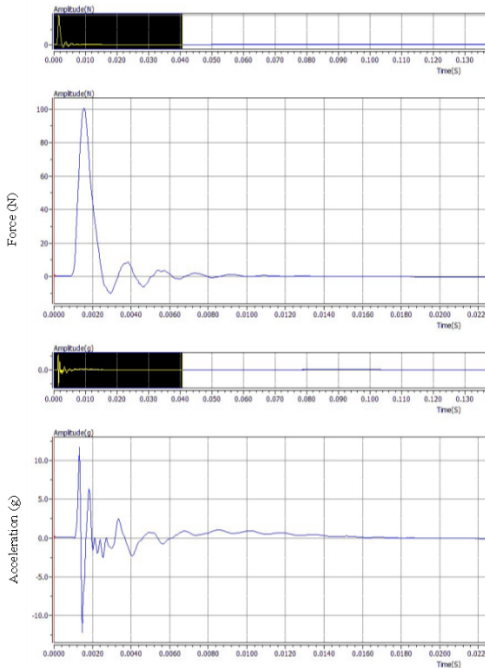


Fig. 7. External excitation force and corresponding acceleration measurement at 0 cycles

Figure 8 shows the FRF phase and magnitude responses at 0 cycles. The phase response (A) oscillates within the frequency range of 0 to 10,000 Hz, with a sharp decrease observed in the range of 1,100 to 3,800 Hz.

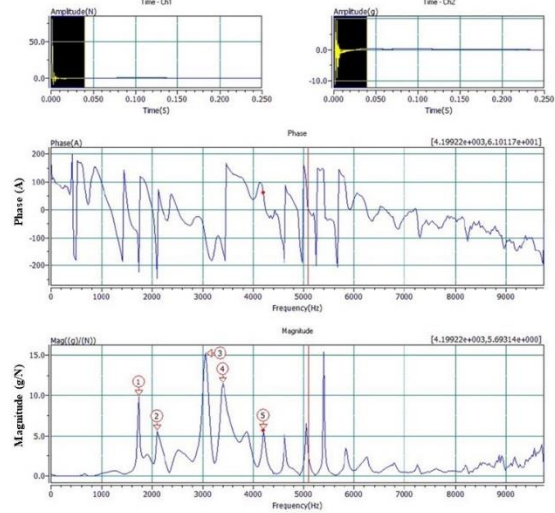


Fig. 8. FRF phase and responses at 0 cycles

Figure 9 shows the FRF and coherence response at 0 cycles. The flat coherence up to 9,000 Hz with a value of 0.9998 indicates that the input and output signals are highly correlated within this frequency range. This high coherence suggests that the vibrational evaluations are reliable, and the experimental setup is effective in capturing the true frequency response of the bone. The maximum oscillation in the magnitude reaching 25 at 5,000 Hz signifies that at this frequency, the bone exhibits the most significant vibrational response. This peak can be used as a diagnostic feature to assess bone health and detect healing progress. Changes in the magnitude response at this and other frequencies over time can provide insights into the structural integrity and healing status of the bone.

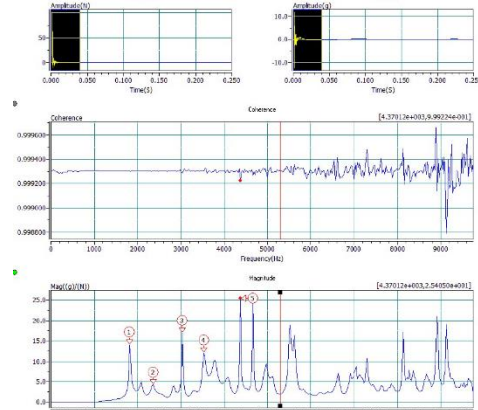


Fig. 9. FRF and coherence response at 0 cycles

Figure 10 provides valuable insights, including the fact that the force reaches 100 N and the acceleration begins at exactly 0.0020 seconds, indicating a direct and immediate response of the bone to the applied force. The acceleration oscillates

from 0.0020s to 0.0040s, showing the bone's vibrational response to the external force.

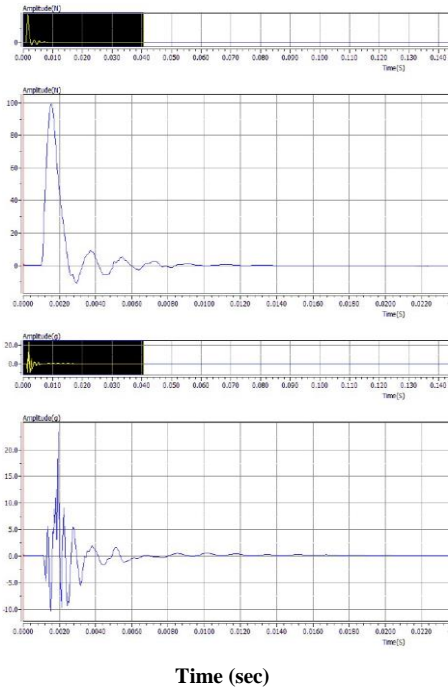


Fig. 10. External excitation force and corresponding acceleration measurement at 1000 cycles

Figure 11 indicates the FRF phase and magnitude responses at 1000 cycles. The phase shows regular oscillations in the phase between 110 and 150 for different frequencies indicate a consistent phase relationship in the bone's response to external excitation. The magnitude peak at 7500 Hz indicates a resonant frequency where the bone's response is most pronounced. Tracking this peak over time can provide valuable information about the changes in bone stiffness and structural integrity as healing progresses.

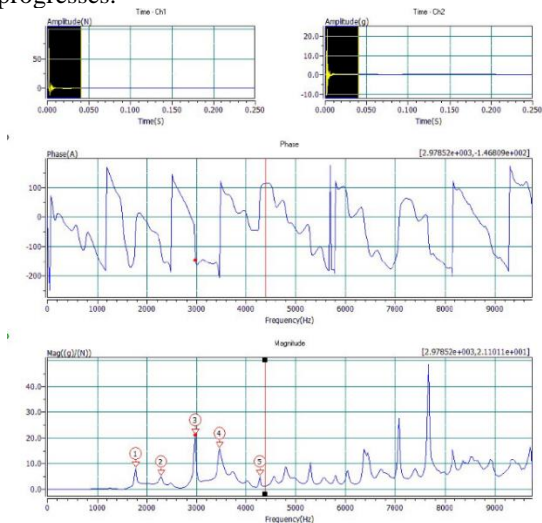


Fig. 11. FRF phase and magnitude responses at 1000 cycles

Figure 12 presents the FRF and coherence response at 1000 cycles. The coherence shows a flat plot up to 6000 Hz, indicating a consistent relationship between the input and output signals within this frequency range. The magnitude peak remains constant, suggesting that the peak rate of the bone's vibrational response does not change across these frequencies."

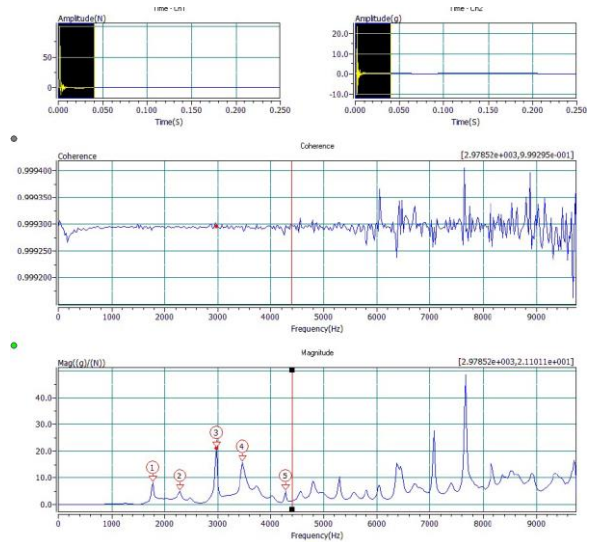


Fig. 12. FRF and coherence response at 1000 cycles

Figure 13 shows the external excitation force and the corresponding acceleration measurement at 2000 cycles. The force peaks at 90 N at 0.0020 seconds, while the acceleration rate remains constant. This consistency in the acceleration response, despite the peak force, supports the reliability of the vibrational measurements.

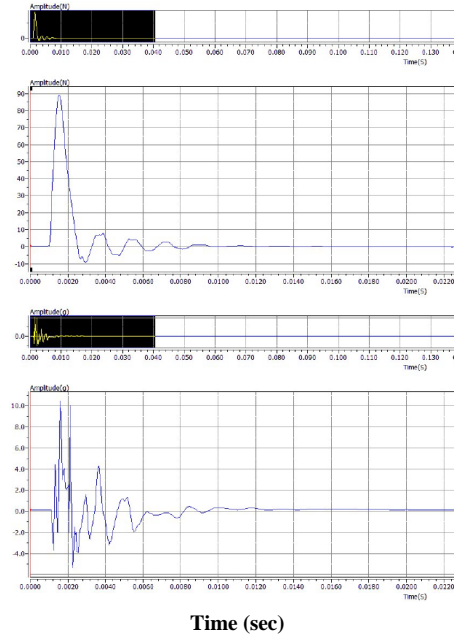


Fig. 13. External excitation force and corresponding acceleration measurement at 2000 cycles

Figure 14 shows the FRF phase and magnitude responses at 2000 cycles. The phase response shows no significant differences across different cycles, while the magnitude peak reaches 8 at 3000 Hz. From 3000 Hz to 6000 Hz, the oscillation in magnitude decreases.

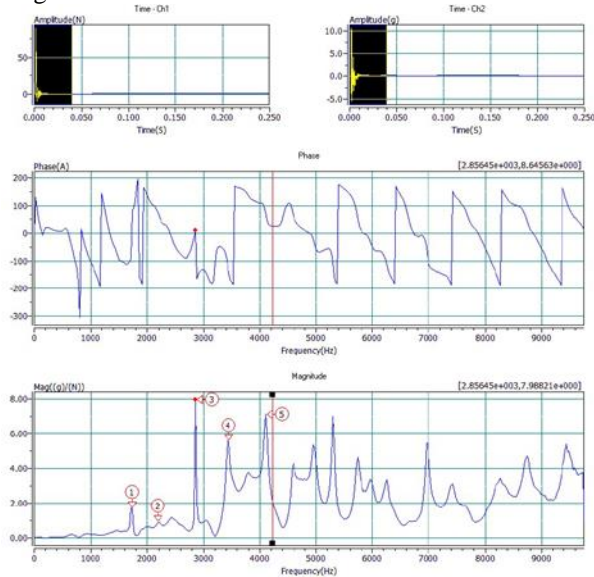


Fig. 14. FRF phase and magnitude responses 2000 cycles

Figure 15 shows the FRF and coherence response at 2000 cycles. The coherence activity begins at 6000 Hz, while the magnitude peak remains consistent throughout the observed frequency range.

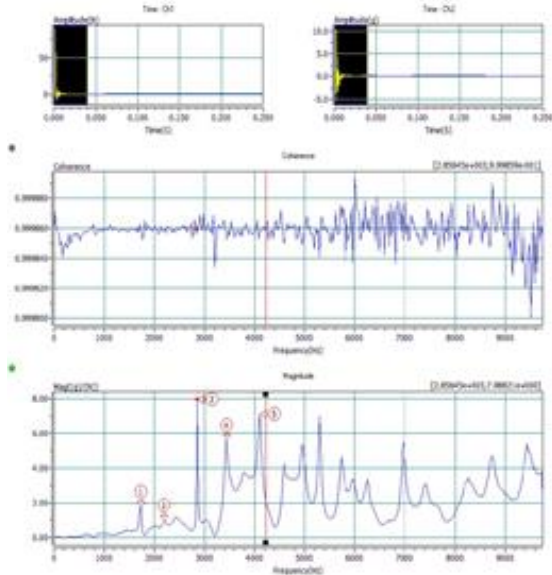


Fig. 15. FRF and coherence response 2000 cycles

Figure 16 shows the external excitation force and corresponding acceleration measurement at 3000 cycles. The force reaches its maximum at 0.0030 seconds and then decreases until 5000 Hz, while the acceleration also reaches 110 at the same time.

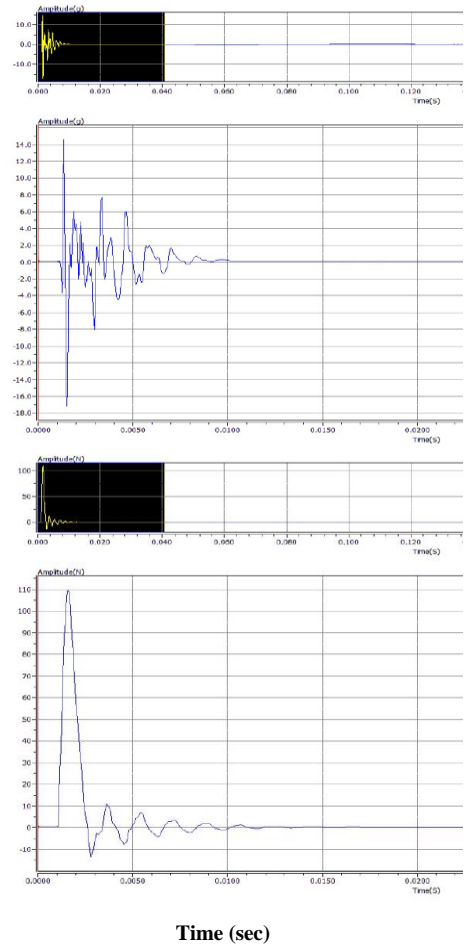


Fig. 16. External excitation force and corresponding acceleration measurement at 3000 cycles

Figure 17 shows the FRF phase and magnitude responses at 3000 cycles. The FRF phase exhibits an unstable rate at different frequencies, while the magnitude response reaches a maximum of 20 at 5000 Hz.

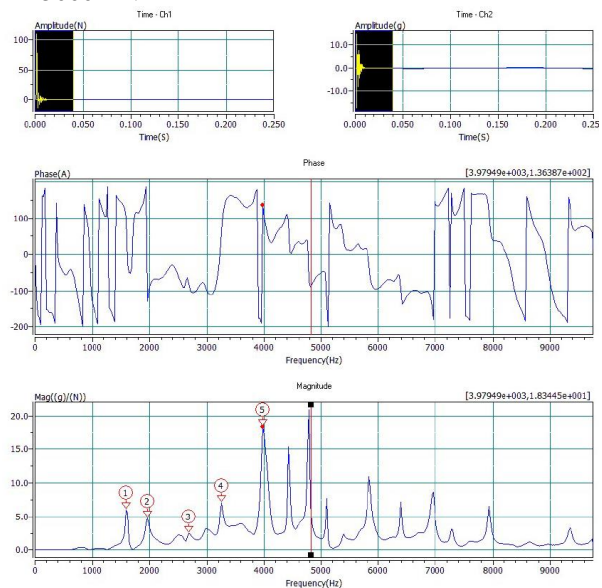


Fig. 17. FRF phase and magnitude responses at 3000 cycles

Figure 18 shows the FRF and coherence response at 3000 cycles. The coherence initially exhibits maximum oscillation between 10 and 50 Hz, then flattens out until 8000 Hz, after which it resumes normal oscillation. Meanwhile, the magnitude response remains consistent throughout.

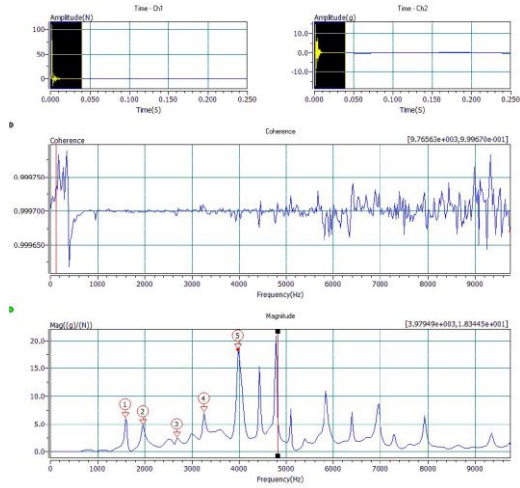


Fig. 18. FRF and coherence response at 3000 cycles

Figure 19 shows the external excitation force and the corresponding acceleration measurement at 4000 cycles. The force reaches 80 N at 0.0030 seconds, while the acceleration extends until 0.01s.

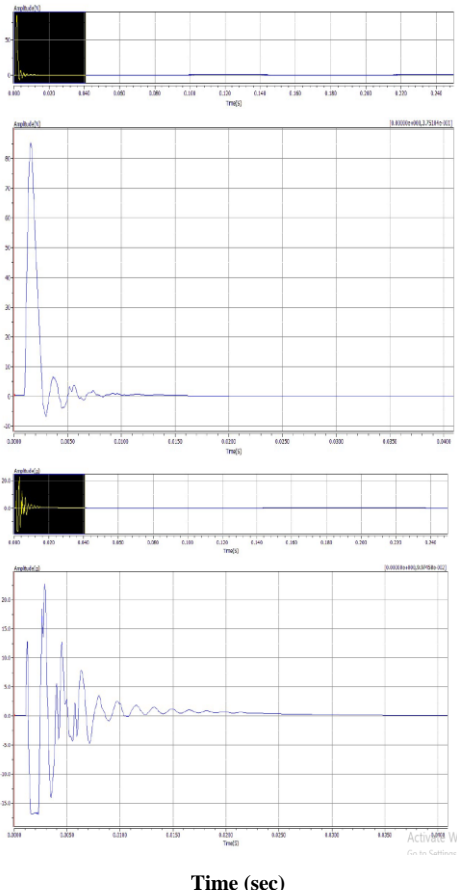


Fig. 19. External excitation force and corresponding acceleration measurement at 4000 cycles

Figure 20 shows the FRF phase and magnitude responses at 4000 cycles. The FRF phase remains consistent across frequencies, while the magnitude response peaks at 30 at 4500 Hz and then flattens out beyond this frequency.

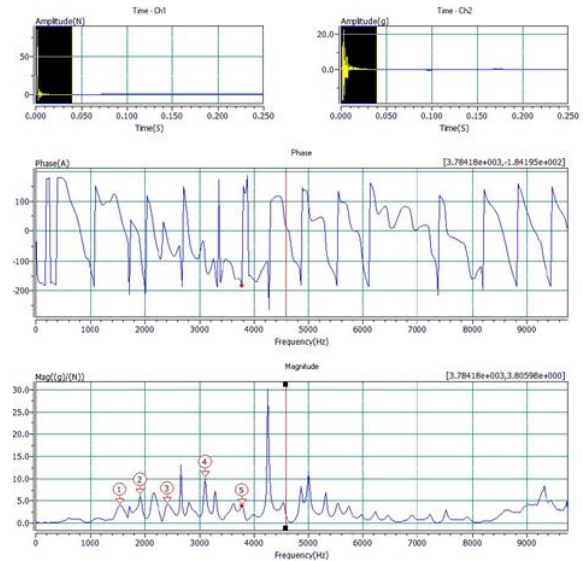


Fig. 20. FRF phase and magnitude responses at 4000 cycles

In Figure 21, the onset of oscillation in coherence from 5000 Hz, peaking at 9000 Hz, indicates that the relationship between the input and output signals becomes more variable and well-defined within this frequency range. This peak in coherence suggests strong signal consistency at higher frequencies, while the magnitude response remains unchanged.

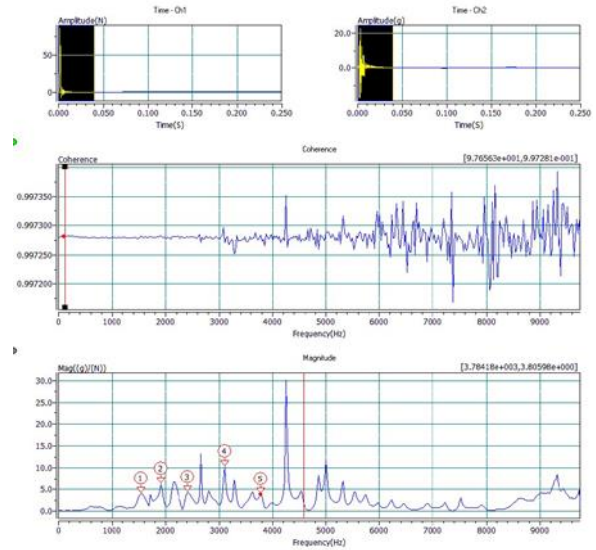


Fig. 21. FRF and coherence response at 4000 cycles

5.3 Natural frequency for all samples at different cycles

When a bone cracks or fractures, its mechanical qualities and behavior change substantially. One factor to consider is natural frequency and its relevance to cyclic loading. In the event of a broken bone, the presence of the crack affects its structural

integrity and natural frequency. The crack functions as a discontinuity, influencing the passage of stress waves through the bone. Resonance is a phenomenon in which the amplitude of vibrations increases dramatically as the applied load frequency synchronizes with the natural frequency of the bones as shown in figures above (red circles). In the case of a cracked bone, resonance might result in high stress concentrations at the break site, potentially causing more damage or delaying healing.

The natural frequencies of the cracked bone for the above sample for five modes will be presented in Table 1. In terms of the relationship between natural frequency and number of cycles, it is vital to remember that cyclic loading can influence a cracked bone natural frequency. As the bone is loaded repeatedly, the crack propagates and change size, affecting the stiffness and overall mechanical behavior. The general trend of the Tables above show that the natural frequency decreasing with increasing the cycles (denoted by the red circle) in the figures above.

An alternative way to comprehend the decreasing of the natural frequencies with modes of the samples with respect of increasing in the number of cycles, the percentage reduction of each mode is calculated by $(Red. (i) = freq_{N=i} - freq_{N=0} / freq_{N=0})$, where $freq_{N=i}$ and $freq_{N=0}$ are the natural frequencies for a specific mode at i and 0 cycles, respectively. Table 2 shows the reduction in the natural frequencies. The maximum values of the reduction for all samples are noticed at the first mode shape and at the maximum number of cycles. There is a reason beyond why the maximum reduction takes place at the first natural frequency and maximum number of cycles. First of all, the spatial distribution of displacement and vibration associated with each natural frequency is described by the mode shapes of the bone. When a bone is fractured, the mode shapes show various patterns of deformation and vibration that take place when the bone is loaded externally. Every mode shape represents a distinct natural frequency; the lowest frequency is represented by the first mode, and the higher frequencies are by the successive modes. When the cracked bone is exposed to cyclic loading that resembles the first mode, the loading conditions and applied forces are largely consistent with the bending behavior associated with the first mode form, which is similar to what have done in this work. This alignment causes the largest stress concentration at the fracture tip during cyclic loading, making it especially vulnerable to changes caused by repeated bending loads. In addition, the stress concentration at the fracture tip plays a vital role in crack propagation and behavior. When cyclic loading is applied, the stress intensity at the fracture tip changes cyclically. These variances can result in fatigue crack development, changes in crack size and form, or fracture closure and reopening. It is well known that the natural frequency of a structure is influenced by its stiffness. The stiffness of the bone

reduces as the fracture grows or spreads, which lowers the natural frequency linked to the first mode. The bone capacity to vibrate at that particular frequency decreases in proportion to the decrease in natural frequency. In contrast to the first mode, the higher modes of vibration have distinct mode geometries and stress distributions. These modes, which usually include several nodes and antinodes, require more intricate patterns of deformation and vibration. In comparison to the first mode, the stress concentration at the fracture tip is often smaller in these higher modes. In the higher modes, the effect of cyclic loading on crack behavior and size changes is often less important because of the lower stress concentration near the fracture tip. As a result, in comparison to the first mode, the natural frequency decrease linked to these higher modes is less.

Table 1. Natural Frequencies (Hz)

Natural Frequencies for sample (S1) at different cycles (N)				
N=0	N=1000	N=2000	N=3000	N=4000
1806.641	1782.227	1733.398	1586.914	1538.086
2368.164	2294.922	2197.266	1953.125	1904.297
3027.344	2978.516	2856.445	2685.547	2419.992
3540.039	3466.797	3442.383	3247.07	3100.586
4370.117	4272.461	4101.563	3979.492	3787.18

Table 2. Percentage reduction in natural frequency

RED.1	RED.1	RED.1	RED.1
-0.01351	-0.04054	-0.12162	-0.14865
-0.03093	-0.07216	-0.17526	-0.19588
-0.01613	-0.05645	-0.1129	-0.20062
-0.02069	-0.02759	-0.08276	-0.12414
-0.02235	-0.06145	-0.08939	-0.13339

Finally, the natural frequency and bone health can be explained in Figure 22. Effect of number of turns on the natural frequency of the first mode only is explained for sample S1.

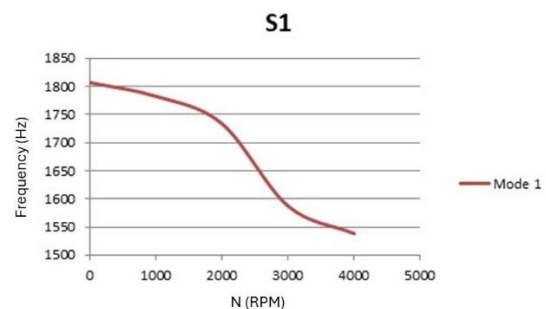


Fig. 22. Effect of cycles number on natural frequency of first mode of S1

Figure 22 shows a decreasing number of cycles rather than an increasing, providing an alternate interpretation of the data. The explanation makes it clear that fewer cycles might provide information about the size of the fracture and, in turn, the health of the bone. The number of cycles and the size and

form of the cracks are directly correlated. A decrease in cycles is correlated with an increase in the bone natural frequency. An improvement in bone health, notably a reduction in crack size, may be indicated by this increasing in natural frequency. One may conclude that the crack size is getting smaller by looking at the number of cycles getting smaller. This tiny fracture indicates a less significant structural flaw in the bone, which is good for the stability and health of the bone. A greater natural frequency results from an increase in bone stiffness as the crack size reduces. Consequently, the decreasing crack size is reflected in the increasing natural frequency, which acts as a sign of better bone health. It is critical to remember that this interpretation is predicated on the notion that the number of cycles, fracture size, and bone shape are proportionately related. Furthermore, the idea that the stiffness and natural frequency increase as crack size decreases underlies the link between natural frequency and crack size. To end up with, natural frequency can be considered as a good indicator about bone health.

6. CONCLUSIONS

The displacement response of the bone closely mirrors the excitation behavior produced by the hammer. However, for instance, in sample S1, the acceleration response persists longer than the excitation forces (0.016 sec). A broken bone's structural integrity and natural frequency are affected by the presence of a crack, as observed from the frequency response results. Specifically, the natural frequency decreases with an increasing number of cycles, with the maximum frequency reduction occurring at the first mode shape and highest number of cycles. This first mode shows the most significant variations in crack behavior because the fracture tip experiences the most force. The observed correlation between decreasing crack size and increasing natural frequency suggests that natural frequency is a reliable indicator of bone health.

Future work should focus on further validating the frequency response method across a broader range of bone types and fracture conditions. Additionally, developing algorithms to automate the assessment of natural frequency and integrating this approach with other diagnostic tools could enhance its clinical applicability. Further studies could also explore the relationship between various crack sizes and natural frequency more deeply to refine this non-invasive method for monitoring bone repair and overall bone health.

Source of funding: *This research received no external funding.*

Author contributions: *research concept and design, A.J.A., M.J.A., A.M.A.-J.; Collection and/or assembly of data, A.J.A., M.J.A., A.M.A.-J.; Data analysis and*

interpretation, A.J.A., M.J.A., A.M.A.-J.; Writing the article, A.J.A., M.J.A., A.M.A.-J.; Critical revision of the article, A.J.A., M.J.A., A.M.A.-J.; Final approval of the article, A.J.A., M.J.A., A.M.A.-J.

Declaration of competing interest: *The authors declare that they have no known competing financial interests or personal relationships that could have appeared to influence the work reported in this paper.*

REFERENCES

- Anderson WD, Wilson SLM, Holdsworth DW. Development of a wireless telemetry sensor device to measure load and deformation in orthopaedic applications. *Sensors* 2020; 20(23): 6772. <https://doi.org/10.3390/s20236772>.
- Joutsen A, Hautalahti J, Jaatinen E, Goebeler S, Paldanius A, Viik J, i in. A device for measuring sternal bone connectivity using vibration analysis techniques. *Proceedings of the Institution of Mechanical Engineers, Part H: Journal of Engineering in Medicine* 2020; 234(1): 81–90. <https://doi.org/10.1177/0954411919884802>.
- Sorriento A, Chiurazzi M, Fabbri L, Scaglione M, Dario P, Ciuti G. A novel capacitive measurement device for longitudinal monitoring of bone fracture healing. *Sensors* 2021; 21(19): 6694. <https://doi.org/10.3390/s21196694>.
- Zou K, Chen Z, Yuan X, Shen X, Wang M, Fu H. A review of uncertainty estimation and its application in medical imaging. *Meta-Radiology* 2023; 1(1): 100003. <https://doi.org/10.1016/j.metrad.2023.100003>.
- Song S, Cheng X, Li T, Shi M, Zheng G, Liu H. Experimental study of bone drilling by Kirschner wire. *Medical Engineering & Physics* 2022; 106: 103835. <https://doi.org/10.1016/j.medengphy.2022.103835>.
- Arpinar P, Simsek B, Sezgin OC, Birlık G, Korkusuz F. Correlation between mechanical vibration analysis and dual energy X-ray absorptiometry (DXA) in the measurement of in vivo human tibial bone strength. *Technology and Health Care: Official Journal of the European Society for Engineering and Medicine* 2005; 13(2): 107–13.
- Christopoulou GE, Stavropoulou A, Anastassopoulos G, Panteliou SD, Papadaki E, Karamanos NK, i in. Evaluation of modal damping factor as a diagnostic tool for osteoporosis and its relation with serum osteocalcin and collagen I N-telopeptide for monitoring the efficacy of alendronate in ovariectomized rats. *Journal of Pharmaceutical and Biomedical Analysis* 2006; 41(3): 891–7. <https://doi.org/10.1016/j.jpba.2005.12.038>.
- Kawchuk GN, Decker C, Dolan R, Fernando N, Carey J. The feasibility of vibration as a tool to assess spinal integrity. *Journal of Biomechanics* 2008; 41(10): 2319–23. <https://doi.org/10.1016/j.jbiomech.2008.04.023>.
- Bediz B, Nevzat Özgüven H, Korkusuz F. Vibration measurements predict the mechanical properties of human tibia. *Clinical Biomechanics* 2010; 25(4): 365–71. <https://doi.org/10.1016/j.clinbiomech.2010.01.002>.
- van Engelen SJPM, Ellenbroek MHM, van Royen BJ, de Boer A, van Dieën JH. Validation of vibration testing for the assessment of the mechanical properties of human lumbar motion segments. *Journal of*

Biomechanics 2012; 45(10): 1753–8.

<https://doi.org/10.1016/j.jbiomech.2012.05.009>.

11. Campoli G, Baka N, Kaptein BL, Valstar ER, Zachow S, Weinans H, i in. Relationship between the shape and density distribution of the femur and its natural frequencies of vibration. *Journal of Biomechanics* 2014; 47(13): 3334–43.
<https://doi.org/10.1016/j.jbiomech.2014.08.008>.
12. Mattei L, Longo A, Di Puccio F, Ciulli E, Marchetti S. vibration testing procedures for bone stiffness assessment in fractures treated with external fixation. *Annals of Biomedical Engineering* 2017; 45(4): 1111–21. <https://doi.org/10.1007/s10439-016-1769-1>.
13. Di Puccio F, Mattei L, Longo A, Marchetti S. Fracture healing assessment based on impact testing: in vitro simulation and monitoring of the healing process of a tibial fracture with external fixator. *International Journal of Applied Mechanics* 2017; 09. <https://doi.org/10.1142/S1758825117500983>.
14. Di Puccio F, Mattei L, Longo A, Marchetti S. Investigation on the feasibility of bone stiffness assessment from in-vivo tests. 2017
15. Mattei L, Di Puccio F, Marchetti S. In vivo impact testing on a lengthened femur with external fixation: a future option for the non-invasive monitoring of fracture healing? *Journal of the Royal Society, Interface* 2018; 15(142): 20180068.
<https://doi.org/10.1098/rsif.2018.0068>.
16. Verdenelli L, Rossetti R, Chiariotti P, Martarelli M, Scalise L. Experimental and numerical dynamic characterization of a human tibia. *Journal of Physics: Conference Series* 2018; 1149(1): 012029.
<https://doi.org/10.1088/1742-6596/1149/1/012029>.
17. Mattei L, Di Puccio F, Marchetti S. Fracture healing monitoring by impact tests: single case study of a fractured tibia with external fixator. *IEEE Journal of Translational Engineering in Health and Medicine* 2019; 7: 2100206.
<https://doi.org/10.1109/JTEHM.2019.2901455>.
18. Chiu WK, Vien BS, Russ M, Fitzgerald M. Towards a non-invasive technique for healing assessment of internally fixated femur. *Sensors (Basel, Switzerland)* 2019; 19(4): 857.
<https://doi.org/10.3390/s19040857>.
19. Mattei L, Di Fonzo M, Marchetti S, Di Puccio F. A quantitative and non-invasive vibrational method to assess bone fracture healing: a clinical case study. *International Biomechanics*; 8(1): 1–13.
<https://doi.org/10.1080/23335432.2021.1874528>.
20. Vien BS, Chiu WK, Russ M, Fitzgerald M. Modal frequencies associations with musculoskeletal components of human legs for extracorporeal bone healing assessment based on a vibration analysis approach. *Sensors* 2022; 22(2): 670.
<https://doi.org/10.3390/s22020670>.
21. Mobark HFH, Fadhel EZ, Hussein MT, Mohamad B. Experimental study of nano-composite materials on vibration responses. *Diagnostyka* 2023; 24(3): 1–13.
<https://doi.org/10.29354/diag/171710>.



Abbas Jawad KADHIM
Mechanical Engineering
Department, College of
Engineering, University of
Babylon, 51001 Babylon, Iraq
E-mail:
mengabbas@gmail.com



**Dr. Mohammed Jawad
AUBAD**
Mechanical Engineering
Department, College of
Engineering, University of
Babylon, 51001 Babylon, Iraq
E-mail:
eng.mahmmedd.jaued@uobabylon.edu.iq



Dr. Ameen M. AL-JUBOORI
Mechanical Engineering
Department, College of
Engineering, University of
Babylon, 51001 Babylon, Iraq
E-mail:
ameenal-juboori@uomus.edu.iq